Distortional Buckling Tests on Cold-Formed Steel Beams

Cheng Yu[1] and Benjamin W. Schafer[2]

Abstract: Failure in cold-formed steel beams is generally initiated by one of three instabilities: local, distortional, or lateral-torsional buckling. For cold-formed steel joists, purlins, or girts, when the compression flange is not restrained by attachment to sheathing or paneling, distortional buckling may be the predominant failure mode. Experimental results on cold-formed steel beams with unrestrained compression flanges are scarce. Therefore a series of distortional buckling tests on cold-formed steel C and Z sections in bending was conducted to establish the capacity in distortional buckling failures. Test details were selected to allow distortional buckling to form, but restrict lateral-torsional buckling to the extent possible. These distortional buckling tests also provide a direct comparison against the local buckling tests previously performed by the writers. As expected, large strength reductions are observed in the tested specimens when distortional buckling initiated the failure instead of local buckling. U.S., Canadian, and joint North American standards for design, which are known to primarily focus on local buckling, provided unconservative predictions of the observed strength. The Australian/New Zealand Standard and the direct strength method, which provide explicit methods for calculating the capacity in the distortional buckling mode, provided reasonably accurate and reliable predictions.

DOI: 10.1061/(ASCE)0733-9445(2006)132:4(515)

CE Database subject headings: Thin wall structures; Steel beams; Buckling; Predictions.

Introduction

Cold-formed steel beams are commonly used in civil construction as both secondary, e.g., girts and purlins, and primary, e.g., floor joists, structural members. This paper focuses on two of the most common sections employed in these applications, the C and Z section. Cold-formed steel C and Z sections are formed from coils of thin metal (on the order of 1 mm thick) and the resulting cross section is thin-walled. Thin-walled members must carefully consider the role of cross-section instability in their design.

Cross-section instabilities in C and Z section beams include: local buckling, distortional buckling, and lateral-torsional buckling. The cross-section deformations associated with each of the three buckling modes are illustrated in Fig. 1. Local buckling involves distortion of the cross section with only rotation occurring at interior fold lines of the section. Distortional buckling involves distortion of the cross section with rotation and translation occurring at interior fold lines. Lateral-torsional buckling excludes distortion of the cross section; however, translation and rotation of the entire cross section occur.

The local, distortional, and lateral-torsional buckling modes also differ greatly in their longitudinal variation along the beam. The longitudinal deformation associated with each of the three buckling modes is sinusoidal with a half-wavelength as identified by the minima in Fig. 1. The local buckling mode occurs with repeated waves at a short length, while lateral-torsional buckling occurs in one half-wave over the unbraced length of the beam. Distortional buckling repeats at a wavelength intermediate to the two other modes.

The moments associated with each of the three buckling modes are given in Fig. 1 as the ratio of the elastic critical buckling moment (M_{cr}) to the moment at first yield (M_y). The minima in Fig. 1 provide the critical values. Determination of the bending strength, for use in design, requires consideration of these cross-section instabilities, as well as the differing postbuckling characteristics in each of the buckling modes, potential interaction amongst the modes, and material yielding.

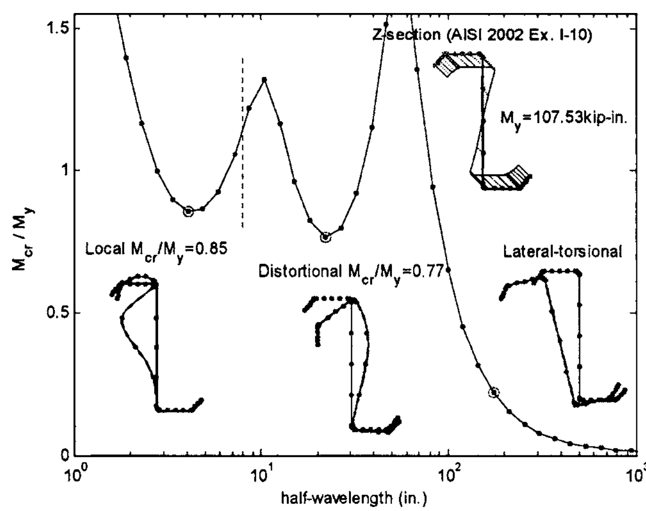

Fig. 1. Buckling modes of a cold-formed steel Z member in restrained bending [restrained bending about a horizontal axis, cross-section designated as 8ZS2.25×059, F_y=380 MPa (55 ksi)]

[1]Assistant Professor, UNT Research Park-Room F115F, Univ. of North Texas, Denton, TX 76207. E-mail: cyu@unt.edu

[2]Assistant Professor, 203 Latrobe Hall, Johns Hopkins Univ., Baltimore, MD 21218. E-mail: schafer@jhu.edu

Note. Associate Editor: Donald W. White. Discussion open until September 1, 2006. Separate discussions must be submitted for individual papers. To extend the closing date by one month, a written request must be filed with the ASCE Managing Editor. The manuscript for this paper was submitted for review and possible publication on February 9, 2005; approved on June 27, 2005. This paper is part of the ***Journal of Structural Engineering***, Vol. 132, No. 4, April 1, 2006. ©ASCE, ISSN 0733-9445/2006/4-515–528/$25.00.

Table 1. Summary of Specimens Selected for Testing

Performed tests	Number	h/t Min.	h/t Max.	b/t Min.	b/t Max.	d/t Min.	d/t Max.	h/b Min.	h/b Max.	d/b Min.	d/b Max.
Group 1 Z: h, $b \sim d$ fixed, t varied	7	71.3	138.2	21.9	39.3	7.0	13.4	3.2	3.6	0.28	0.37
Group 2 Z: h, $b \sim d$ fixed, t varied	2	126.6	140.4	38.6	42.0	10.1	11.5	3.2	3.3	0.26	0.28
Group 3 C: h, b d fixed, t varied	8	80.7	241.7	20.3	59.1	6.4	20.3	3.8	4.1	0.26	0.35
Group 4 C: b, d fixed, h, t varied	7	66.9	186.7	30.9	43.1	6.4	12.9	2.0	6.0	0.19	0.31
Total	24	66.9	241.7	20.3	59.1	6.4	20.3	2.0	6.0	0.19	0.37

Note: Min.=minimum and Max.=maximum.

North American specifications for cold-formed steel (CSA 1994; AISI 1996; 2001) apply an effective width approach for determining the design strength of beams. First an empirical beam strength curve is used to account for lateral-torsional buckling. Then, to include interaction between lateral-torsional buckling and the other modes, the gross section modulus is reduced to an effective section modulus by performing an element by element reduction via Winter's effective width formula. This element by element effective width reduction accounts for local buckling, and in part, distortional buckling.

The effective width reductions for the AISI (1996) and S136 (CSA 1994) specifications were based primarily on the experimental results of Desmond et al. (1981). Subsequent experiments on laterally braced C and Z beams indicated that the AISI (1996) and S136 (CSA 1994) specifications do not always provide consistent and conservative predictions [e.g., see Hancock et al. (1996); and Schafer and Peköz (1999)]. The two key shortcomings identified were lack of a consistent treatment for the interaction of elements in local buckling, and inadequate provisions to handle distortional buckling. Schafer and Trestain (2002) proposed a modification, adopted in AISI (2001), to partially account for interaction of elements (e.g., the web and flange) in local buckling. In addition, testing focused solely on the local buckling limit state in C and Z sections was completed by Yu and Schafer (2003).

Distortional buckling remains unaddressed as a separate limit state in the North American Specification (AISI 2001). However, based on the work of Hancock (1997) distortional buckling is considered in Australia (AS/NZS 1996). Hancock's method requires calculation of the elastic distortional buckling mode,

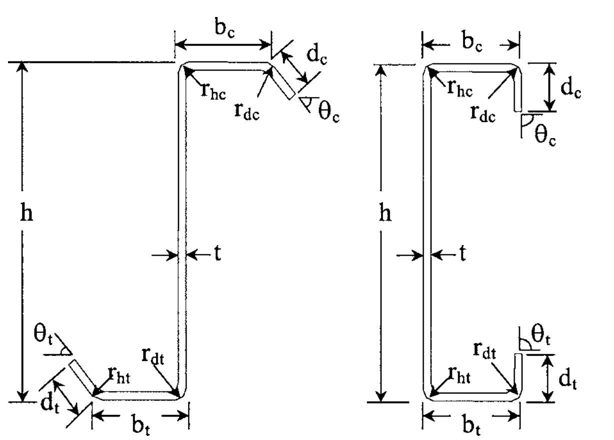

Fig. 2. Definitions for specimen dimensions of C and Z sections

which may be completed using finite strip analysis as given in Fig. 1, or using a closed-form solution (Hancock 1997). Schafer and Peköz (1999) modified Hancock's closed-form solution to cover members in which distortional buckling initiates in the web. Silvestre and Camotim (2004) have supplied an alternative closed-form solution for elastic distortional buckling based on generalized beam theory.

One reason for the lack of an explicit check on distortional buckling in AISI (2001) is that definitive experiments do not exist. The original tests of Desmond et al. (1981) used back-to-back specimens which increased the web stiffness. Subsequent tests by researchers [e.g., see the summary in Schafer and Peköz (1999)] included intermittently spaced angles or through-fastened decking attached to the compression flange. These testing details restrain the distortional buckling mode. This partially masks any problem with AISI (2001) predictions, and also makes existing distortional buckling design methods (e.g., AS/NZS 1996) appear overly conservative. However, design situations do exist when the compression flange is unrestrained. For example, negative bending of continuous members (joists, purlins, etc.) and wind suction on walls and panels without interior sheathing. Experiments focused on unrestrained distortional buckling failures are needed.

An objective of this work is to determine the experimental strength for unrestrained distortional buckling of C and Z sections. Flexural members were chosen for testing, as opposed to compression members, because distortional buckling is a more likely mode of failure in standard C and Z sections under flexure. In axial compression of common C and Z sections, local buckling, initiated in the web, typically occurs in advance of distortional buckling (Schafer 2002). In flexure, as shown in Fig. 1, the stress gradient in the web increases the local buckling moment, and distortional buckling often controls.

Distortional Buckling Tests

A series of four-point bending tests were conducted on industry standard C and Z beams. The details of the tests were selected so that distortional buckling is free to form. The geometry of the selected specimens, testing protocols, and results are explained in the following sections.

Selection of Specimens

C and Z sections commonly used in the cold-formed steel industry were selected for testing. Table 1 summarizes the range of specimens considered and the manner in which variation among

Table 2. Geometry and Material Properties for Distortional Buckling Tests

Group number	Test label	Specimen	h (mm)	b_c (mm)	d_c (mm)	θ_c (deg)	b_t (mm)	d_t (mm)	θ_t (deg)	r_{hc} (mm)	r_{dc} (mm)	r_{ht} (mm)	r_{dt} (mm)	t (mm)	f_y (MPa)	f_u (MPa)
1	D8.5Z120-4E1W	D8.5Z120-4	214	67	24	54.2	63	25	50.2	9	9	9	9	3.00	422.7	572.6
		D8.5Z120-1	214	67	24	48.1	64	25	52.1	9	9	9	9	3.00	426.4	573.7
	D8.5Z115-1E2W	D8.5Z115-2	217	65	23	49.0	61	23	48.3	9	9	9	9	2.97	441.9	577.9
		D8.5Z115-1	216	68	21	48.3	63	22	48.3	9	9	10	10	2.96	453.3	583.4
	D8.5Z092-3E1W	D8.5Z092-3	213	66	24	51.9	61	24	51.6	7	7	8	8	2.27	396.8	497.0
		D8.5Z092-1	214	66	24	52.4	61	24	50.9	7	7	8	8	2.28	397.9	500.1
	D8.5Z082-4E3W	D8.5Z082-4	215	64	24	48.5	61	25	51.3	7	7	8	8	2.06	407.9	510.0
		D8.5Z082-3	216	64	24	49.9	60	24	49.5	7	7	8	8	2.06	406.4	508.8
	D8.5Z065-7E6W	D8.5Z065-7	216	63	21	50.0	63	21	49.3	8	8	9	9	1.63	429.6	575.1
		D8.5Z065-6	217	63	22	53.0	62	21	48.3	8	8	9	9	1.64	436.4	574.4
	D8.5Z065-4E5W	D8.5Z065-5	216	60	17	51.3	64	23	47.2	7	7	7	7	1.64	432.6	573.5
		D8.5Z065-4	213	61	21	47.3	57	16	51.2	8	8	7	7	1.57	401.4	540.5
	D8.5Z059-6E5W	D8.5Z059-6	214	62	20	50.4	61	22	48.0	8	8	8	8	1.57	403.4	545.1
		D8.5Z059-5	216	61	20	48.3	61	19	48.3	8	8	8	8	1.56	406.8	547.1
2	D11.5Z092-3E4W	D11.5Z092-4	285	88	24	48.7	87	23	49.6	8	8	8	8	2.10	481.6	619.5
		D11.5Z092-3	286	87	23	49.3	88	22	49.5	8	8	8	8	2.26	483.1	621.8
	D11.5Z082-3E4W	D11.5Z082-4	290	87	22	48.4	86	22	49.9	8	8	8	8	2.06	507.4	642.2
		D11.5Z082-3	288	87	24	50.2	87	24	51.0	8	8	8	8	2.08	494.7	634.0
3	D8C097-7E6W	D8C097-7	207	55	16	80.8	54	16	80.0	7	7	7	8	2.54	586.9	625.4
		D8C097-6	207	53	16	81.0	53	16	80.0	7	7	7	8	2.55	587.5	632.6
	D8C097-5E4W	D8C097-5	205	51	17	86.7	51	17	83.0	7	8	7	7	2.54	576.9	625.2
		D8C097-4	205	52	17	83.0	51	17	83.0	7	7	7	7	2.53	579.8	627.5
	D8C085-2E1W	D8C085-2	205	50	16	86.0	50	17	86.6	6	6	6	6	2.10	363.8	453.7
		D8C085-1	205	50	16	88.6	50	17	89.0	6	5	6	5	2.15	357.2	442.1
	D8C068-6E7W	D8C068-6	202	49	17	80.0	50	16	77.8	4	4	4	4	1.80	543.9	557.2
		D8C068-7	202	50	16	76.5	50	17	77.5	4	4	4	4	1.80	550.3	556.4
	D8C054-7E6W	D8C054-7	204	52	14	83.4	52	14	88.7	6	6	5	6	1.34	281.2	361.9
		D8C054-6	203	52	15	89.4	52	14	83.3	6	6	6	6	1.32	280.3	350.4
	D8C045-1E2W	D8C045-1	208	49	17	89.0	49	17	87.6	7	5	6	5	0.88	147.3	294.0
		D8C045-2	207	49	17	88.8	49	18	88.3	7	5	6	5	0.88	144.9	293.8
	D8C043-4E2W	D8C043-4	204	51	13	87.3	51	14	88.8	4	5	4	5	1.17	313.1	420.6
		D8C043-2	204	51	13	88.9	50	14	87.7	5	5	5	5	1.20	313.3	420.4
	D8C033-1E2W	D8C033-2	207	51	17	87.1	49	16	85.8	4	8	5	8	0.86	141.0	289.0
		D8C033-1	205	51	16	86.0	50	20	88.0	5	7	5	7	0.86	140.2	290.7
4	D12C068-10E11W	D12C068-11	306	52	13	82.0	51	14	85.3	6	6	6	6	1.64	226.7	392.2
		D12C068-10	306	51	14	85.9	50	13	94.8	6	6	7	6	1.65	239.1	391.0
	D12C068-1E2W	D12C068-2	303	52	13	82.5	52	15	77.4	7	6	6	6	1.69	388.0	507.7
		D12C068-1	304	54	13	80.6	51	14	83.3	6	6	7	7	1.70	384.9	507.2
	D10C068-4E3W	D10C068-4	256	51	12	83.2	53	14	83.3	7	5	6	6	1.59	151.7	277.4
		D10C068-3	257	53	14	80.7	53	13	81.9	6	6	6	6	1.61	155.3	281.6
	D10C056-3E4W	D10C056-3	254	50	17	88.0	49	16	89.0	3	4	3	3	1.45	532.4	553.8
		D10C056-4	254	49	18	88.6	49	17	87.7	3	4	3	5	1.45	530.0	562.3
	D10C048-1E2W	D10C048-1	253	52	16	86.1	49	16	79.6	5	5	5	5	1.21	351.9	403.3
		D10C048-2	253	51	16	85.7	49	16	83.7	5	5	5	5	1.24	348.8	398.0
	D6C063-2E1W	D6C063-2	152	51	16	88.7	50	16	87.3	5	4	5	6	1.47	385.4	460.1
		D6C063-1	152	51	16	87.0	50	16	86.1	6	4	6	4	1.42	398.4	478.6
	D3.62C054-3E4W	D3.62C054-4	95	48	10	87.0	48	11	89.0	7	6	7	7	1.41	221.2	369.0
		D3.62C054-3	95	48	9	88.0	47	9	88.0	6	7	7	7	1.41	226.8	367.4

Note: Typical specimen label is DxZ(or C)xxx-x. For example, D8.5Z120-1 means the specimen is 216 mm (8.5 in.) high for the web, Z-section, 3.05 mm (0.12 in.) thick and the beam number is 1. Typical test label is DxZ(or C)xxx-xExW. For example, test D8.5Z120-4E1W means the two-paired specimens are D8.5Z120-4 at the east side and D8.5Z120-1 at the west side.

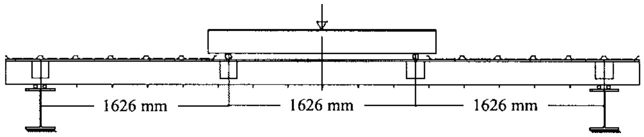

Fig. 3. Elevation view of overall test arrangement for distortional buckling tests

the key nondimensional parameters: web slenderness (h/t), flange slenderness (b/t), lip slenderness (d/t), and web height-to-flange width ratio (h/b), was performed. The dimensions of the specimens (Fig. 2) were recorded at midlength and mid-distance between the center and loading points, for a total of three measurement locations for each specimen. Mean specimen dimensions are provided in Table 2.

Testing Setup

The 4.9 m long four-point bending test consists of two C or Z sections in parallel loaded at the 1/3 points, as shown in Figs. 3 and 4. The compression flanges of the specimens are unconnected in the constant moment span, but connected by a through-fastened panel (0.48 mm thick, 32 mm high at the rib) in the shear spans. The tension flange of the specimens is connected by an intermittently spaced $32 \times 32 \times 1.45$ mm angle attached every 305 mm along the length. Short hot-rolled tube sections $(254 \times 191 \times 152 \times 6$ mm) stiffen and bolt the two specimens together at the ends and load points to minimize shear and web crippling problems. The objective of the testing setup is to allow distortional buckling to form in the constant moment span, while restricting lateral-torsional buckling, and avoiding other limit states.

The loading system employs an 89 kN MTS actuator, which has a maximum 152 mm stroke. The test was performed in displacement control at a rate of 0.0381 mm/s. An MTS 407 controller and load cell monitored the force and insured the desired displacement control was met. Specimen deflections were

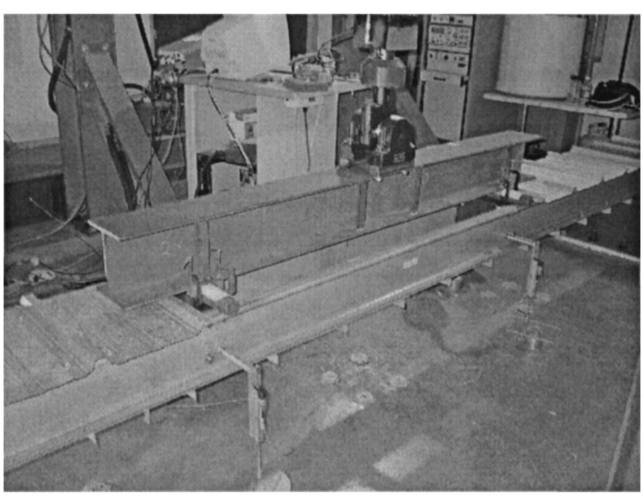

Fig. 4. Panel setup for distortional buckling tests

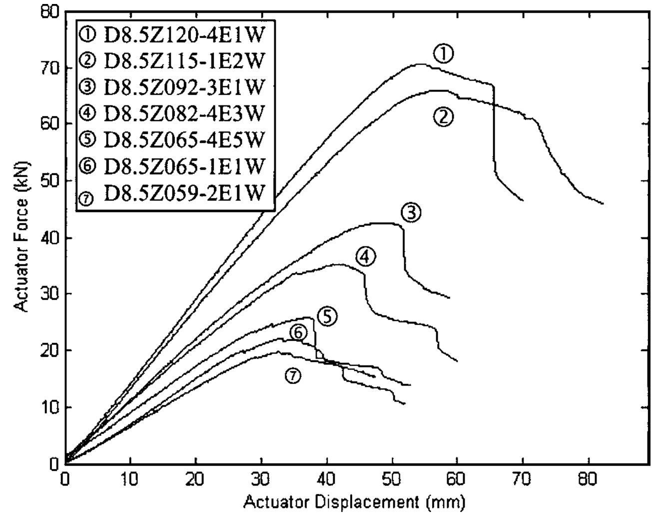

Fig. 5. Actuator force-displacement response of distortional buckling tests—Group 1

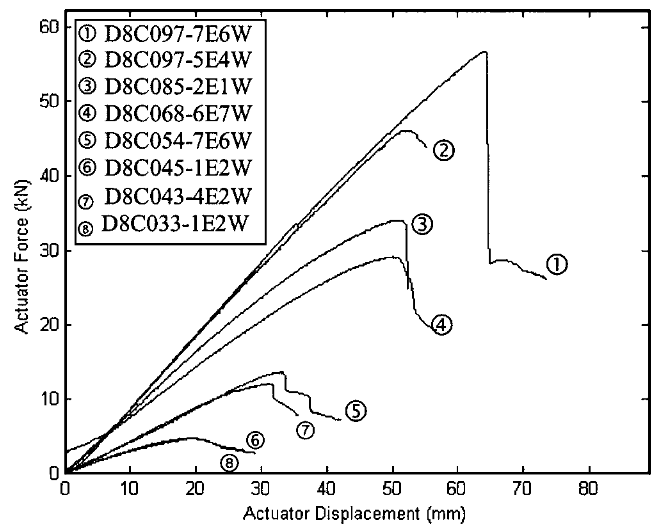

Fig. 6. Actuator force-displacement response of distortional buckling tests—Group 2

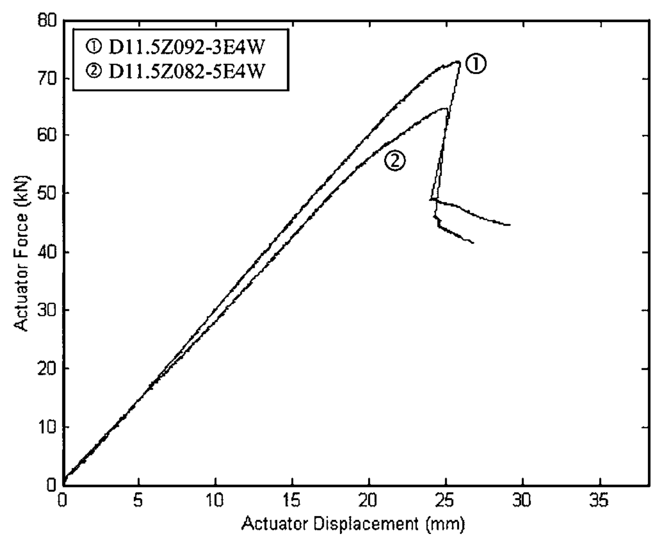

Fig. 7. Actuator force-displacement response of distortional buckling tests—Group 3

Table 3. Distortional Buckling Test Results

Group number	Test label	Specimen	M_{test} (kN m)	M_y (kN m)	$M_{cr\ell}$ (kN m)	M_{crd} (kN m)	M_{test}/M_y	M_{test}/M_{AISI}	M_{test}/M_{S136}	M_{test}/M_{NAS}	$M_{test}/M_{AS/NZS}$	M_{test}/M_{EN1993}	$M_{test}/M_{DS\ell}$	M_{test}/M_{DSd}
1	D8.5Z120-4E1W	D8.5Z120-4[a]	28.7	29.9	83.0	44.2	0.96	0.95	0.95	0.95	1.08	1.00	0.96	1.08
		D8.5Z120-1	28.7	30.4	83.6	40.9	0.94	0.93	0.93	0.93	1.09	1.00	0.94	1.09
	D8.5Z115-1E2W	D8.5Z115-2	26.8	30.6	80.4	41.0	0.88	0.86	0.86	0.86	1.02	0.92	0.88	1.02
		D8.5Z115-1[a]	26.8	31.6	78.3	37.5	0.85	0.88	0.88	0.88	1.03	0.93	0.85	1.03
	D8.5Z092-3E1W	D8.5Z092-3[a]	17.3	21.0	36.7	23.6	0.82	0.83	0.85	0.82	1.01	0.88	0.82	1.01
		D8.5Z092-1	17.3	21.2	37.1	23.7	0.82	0.83	0.85	0.83	1.00	0.87	0.82	1.00
	D8.5Z082-4E3W	D8.5Z082-4[a]	14.3	19.9	27.1	18.4	0.72	0.77	0.81	0.76	0.95	0.83	0.77	0.95
		D8.5Z082-3	14.3	19.8	27.1	18.7	0.72	0.77	0.81	0.76	0.94	0.83	0.77	0.94
	D8.5Z065-7E6W	D8.5Z065-7[a]	10.5	16.5	13.3	10.7	0.64	0.75	0.82	0.75	0.96	0.93	0.81	0.96
		D8.5Z065-6	10.5	16.8	13.6	11.6	0.63	0.72	0.79	0.72	0.92	0.88	0.79	0.92
	D8.5Z065-4E5W	D8.5Z065-5	9.0	16.2	12.3	9.9	0.56	0.70	0.75	0.70	0.86	0.83	0.72	0.86
		D8.5Z065-4[a]	9.0	13.8	12.1	9.4	0.65	0.72	0.80	0.72	0.97	0.90	0.80	0.97
	D8.5Z059-6E5W	D8.5Z059-6[a]	8.0	14.6	11.7	9.5	0.55	0.65	0.71	0.65	0.83	0.80	0.70	0.83
		D8.5Z059-5	8.0	14.7	11.6	9.4	0.55	0.64	0.70	0.64	0.83	0.79	0.69	0.83
2	D11.5Z092-3E4W	D11.5Z092-4	29.6	45.4	34.6	23.8	0.65	0.85	0.92	0.85	1.07	1.15	0.84	1.07
		D11.5Z092-3[a]	29.6	45.7	34.2	23.4	0.65	0.86	0.93	0.86	1.07	1.07	0.84	1.07
	D11.5Z082-3E4W	D11.5Z082-4[a]	26.4	44.5	26.0	19.1	0.59	0.86	0.91	0.86	1.06	1.03	0.84	1.06
		D11.5Z082-3	26.4	43.7	26.8	20.7	0.60	0.84	0.89	0.84	1.03	1.02	0.84	1.03
3	D8C097-7E6W	D8C097-7	23.1	28.4	44.6	32.5	0.81	0.85	0.88	0.85	0.99	0.90	0.83	0.99
		D8C097-6[a]	23.1	28.2	44.3	32.8	0.82	0.85	0.89	0.85	0.99	0.91	0.83	0.99
	D8C097-5E4W	D8C097-5[a]	18.7	26.5	42.6	33.5	0.71	0.73	0.76	0.76	0.84	0.77	0.71	0.84
		D8C097-4	18.7	26.9	43.4	33.5	0.69	0.72	0.74	0.72	0.83	0.75	0.70	0.83
	D8C085-2E1W	D8C085-2[a]	13.8	14.0	24.3	21.6	0.99	0.99	1.02	1.02	1.09	1.03	0.99	1.10
		D8C085-1	13.8	14.0	26.2	22.9	0.98	0.98	1.01	1.01	1.07	1.02	0.98	1.07
	D8C068-6E7W	D8C068-6	11.8	17.8	15.6	15.7	0.67	0.76	0.85	0.83	0.89	0.84	0.82	0.89
		D8C068-7[a]	11.8	18.2	15.8	15.1	0.65	0.77	0.86	0.84	0.89	0.85	0.80	0.89
	D8C054-7E6W	D8C054-7	5.5	6.9	6.5	7.0	0.79	0.86	0.96	0.85	1.01	0.98	0.95	1.01
		D8C054-6[a]	5.5	6.8	6.3	7.5	0.80	0.86	0.95	0.85	1.00	0.98	0.97	0.99
	D8C045-1E2W	D8C045-1	1.9	2.5	1.9	3.8	0.75	0.76	0.84	0.83	0.83	0.90	0.96	0.84
		D8C045-2[a]	1.9	2.4	1.9	3.9	0.77	0.77	0.86	0.85	0.85	0.91	0.98	0.84
	D8C043-4E2W	D8C043-4[a]	4.8	6.7	4.2	5.3	0.72	0.90	0.97	0.90	1.00	1.03	0.99	1.01
		D8C043-2	4.8	6.9	4.6	5.6	0.70	0.86	0.94	0.94	0.98	0.98	0.95	0.97
	D8C033-1E2W	D8C033-2	1.8	2.3	1.7	3.7	0.82	0.82	0.91	0.90	0.90	0.97	1.05	0.89
		D8C033-1[a]	1.8	2.3	1.7	3.3	0.81	0.82	0.91	0.91	0.93	1.00	1.04	0.92
4	D12C068-10E11W	D12C068-11[a]	10.7	12.1	9.5	10.1	0.88	0.92	1.05	1.05	1.21	1.13	1.12	1.21
		D12C068-10	10.7	12.7	9.8	10.7	0.84	0.88	1.00	1.00	1.15	1.07	1.08	1.15
	D12C068-1E2W	D12C068-2[a]	11.1	21.2	10.4	11.0	0.52	0.67	0.72	0.70	0.86	0.79	0.79	0.86
		D12C068-1	11.1	21.3	10.9	11.4	0.52	0.67	0.72	0.70	0.85	0.78	0.77	0.85
	D10C068-4E3W	D10C068-4[a]	5.8	6.0	9.3	9.6	0.95	0.95	1.01	1.01	1.05	1.01	0.98	1.05
		D10C068-3	5.8	6.4	10.0	10.8	0.90	0.90	0.94	0.95	0.96	0.94	0.91	0.97
	D10C056-3E4W	D10C056-3[a]	9.6	19.6	7.4	10.2	0.49	0.71	0.74	0.74	0.81	0.79	0.80	0.81
		D10C056-4	9.6	19.5	7.5	10.9	0.49	0.69	0.72	0.72	0.79	0.76	0.80	0.79
	D10C048-1E2W	D10C048-1[a]	7.0	10.8	4.5	6.7	0.65	0.86	0.90	0.90	1.00	1.00	1.03	1.00
		D10C048-2	7.0	10.9	4.7	7.0	0.64	0.85	0.89	0.89	0.98	0.97	1.01	0.98
	D6C063-2E1W	D6C063-2	5.9	7.0	9.8	8.8	0.85	0.94	0.99	0.92	1.00	0.85	0.89	1.00
		D6C063-1[a]	5.9	7.0	8.9	8.0	0.85	0.95	1.01	0.94	1.03	0.85	0.92	1.03
	D3.62C054-3E4W	D3.62C054-4	1.9	1.9	7.9	4.0	1.04	1.08	1.08	1.08	1.07	1.08	1.04	1.05
		D3.62C054-3[a]	1.9	1.9	7.8	3.4	1.04	1.14	1.14	1.11	1.12	1.10	1.04	1.09

[a]Controlling specimen, weaker capacity by AISI (1996).

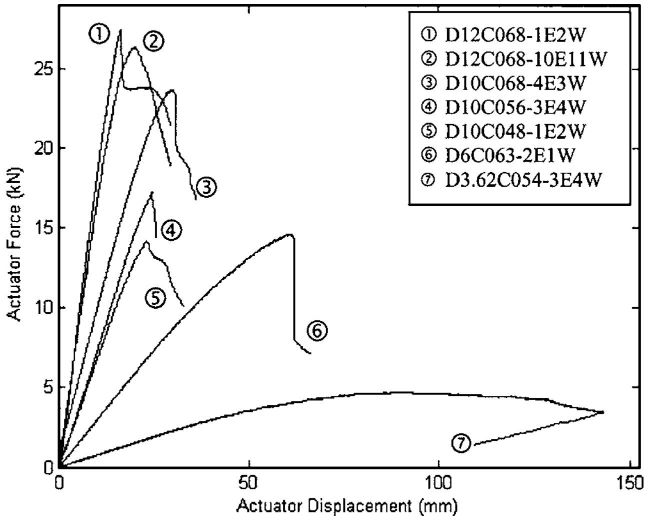

Fig. 8. Actuator force-displacement response of distortional buckling tests—Group 4

measured at the 1/3 points with position transducers. Additional details of the testing setup may be found in Yu and Schafer (2003) and Yu (2005).

Tension Coupon Tests

Tension tests were carried out following the provisions of *ASTM E8-00, standard test methods for tension testing of metallic material* (ASTM 2000). Three tensile coupons were taken from the end of each specimen: one from the web flat, one from the compression flange flat, and one from the tension flange flat. A screw-driven ATS 900, with a maximum capacity of 44.5 kN was used for the loading. An MTS 634.11E-54 extensometer was employed to monitor the deformation.

Coupon test results are summarized in Table 2. Greater variation in the yield stress and ultimate-to-yield (f_u/f_y) ratios was observed in the C sections than in the Z sections. Yield stress in the C sections varied from 140 to 587 MPa, with a range of f_u/f_y ratios from 1.01 (for a high yield stress material) to 2.07 (for a low yield stress material). Yield stress in the Z sections varied from 401 to 495 MPa, while the f_u/f_y ratio was near 1.3 for all specimens. The elastic modulus, E, is assumed to be 203 GPa [see the tension tests conducted by Yu and Schafer (2003) for further discussion of this issue].

Test Results

Table 3 provides a numerical summary of the 24 four-point bending tests that were conducted. Included in Table 3 is the peak moment observed in each test (M_{test}), the moment to cause first yield in each specimen based on the tensile coupon results for that specimen (M_y), and the elastic critical local buckling moment ($M_{\text{cr}\ell}$) and distortional buckling moment (M_{crd}) as determined from a finite strip analysis [*CUFSM*, Schafer (2005), similar to Fig. 1]. In addition, Table 3 also provides ratios of test-to-analytically predicted capacities using design methods, including: the American Specification, M_{AISI} (AISI 1996); the Canadian Standard, M_{S136} (CSA 1994); the North American Specification, M_{NAS} (AISI 2001); the Australia/New Zealand Standard, $M_{\text{AS/NZS}}$ (AS/NZS 1996); the European Standard EN1993, M_{EN1993} (CEN 2002); and the direct strength method (DSM), Schafer and Peköz 1998; AISI 2004: Appendix 1—$M_{\text{DS}\ell}$ for local failures, M_{DSd} for distortional failures). Figs. 5–8 provide the actuator load-displacement response for the 24 tests. The response is broken into the four different geometric groups summarized in Table 1. The test results and interpretations are discussed in detail in the subsequent sections.

Comparison with Local Buckling Tests

The distortional buckling tests reported in this paper provide an opportunity for comparison with the local buckling tests conducted by Yu and Schafer (2003). The setup for the two series of tests is identical, except in the distortional buckling tests the compression flange is unrestrained in the constant moment span, and in the local buckling tests the compression flange is restrained by a specially detailed through-fastened deck. Fig. 9 provides the observed buckling modes in a local and a distortional buckling test for nominally identical specimens. In the distortional buckling test the buckling wavelength is visibly longer and the compression flange rotates about the web/compression flange junction. The observed strength is also significantly reduced.

Among 25 local buckling and 24 distortional buckling tests, nine pairs of tests use beams with nominally identical geometry and material. The observed capacity of these nine tests

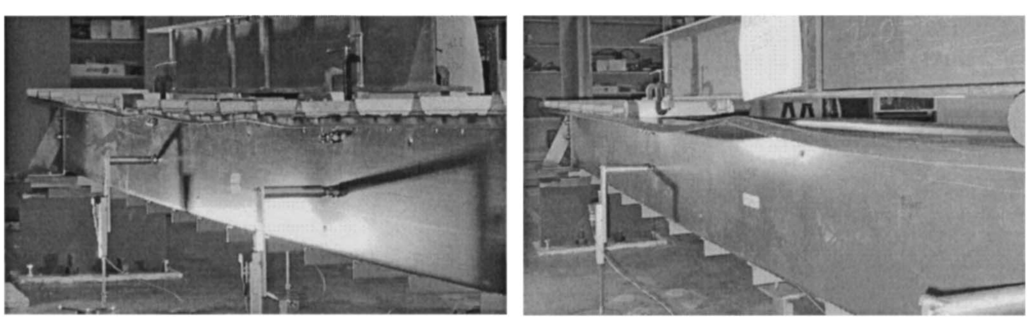

(a) Local buckling test of 11.5Z092-1E2W (b) Distortional buckling test of D11.5Z092-3E4W

Fig. 9. Comparison of local buckling and distortional buckling tests for 11.5Z092

Table 4. Comparison of Nine Pairs of Tests Having the Same Nominal Geometry and Material Properties

Pair number	Local buckling test label	Distortional buckling test label	Actuator peak load of local test P_L (kN)	Actuator peak load of distortional test P_D (kN)	P_D/P_L (%)
1	8.5Z120-3E2W	D8.5Z120-4E1W	77.93	70.59	91
2	8.5Z092-4E2W	D8.5Z092-3E1W	50.40	42.55	84
3	8.5Z082-1E2W	D8.5Z082-4E3W	45.06	35.23	78
4	8.5Z059-2E1W	D8.5Z059-4E3W	27.49	19.75	72
5	8C054-1E8W	D8C054-7E6W	15.53	13.49	87
6	8C043-5E6W	D8C043-4E2W	14.21	11.91	84
7	12C068-3E4W	D12C068-1E2W	38.00	27.40	72
8	12C068-9E5W	D12C068-10E11W	28.94	26.30	91
9	3.62C054-1E2W	D3.62C054-3E4W	5.62	4.76	85
				Average	83

is provided in Table 4. On average the distortional buckling tests result in a 17% reduction in the capacity of the section when compared with the local buckling test.

For a typical Z section (8.5Z092) the actuator load-displacement response and observed failure mechanism in the two tests are provided in Figs. 10 and 11. The load-displacement response also includes notations for the actuator load which causes first yield in the specimen (P_y) as well as the actuator load for elastic critical local buckling (P_{crL}) and distortional buckling (P_{crD}) as determined from finite strip analysis. For this Z section, and many of the tested specimens, the response is in the inelastic regime, i.e., the elastic local buckling loads (moments) are above that to cause first yield. The elastic stiffness is the same in the local and distortional buckling tests, but the distortional buckling tests fails at a lower load and with a slight increase in nonlinearity, as shown in Fig. 10. In the distortional buckling test, the deformations that trigger failure exhibit longer wavelengths in the flange, and little deformation in the web, when compared to the local buckling tests.

For a typical C section (8C043) the actuator load-displacement response and observed failure mechanism in the two tests are provided in Figs. 12 and 13. The elastic stiffness in the local and distortional buckling tests is the same, but failure occurs earlier in the distortional buckling test. Interestingly, in the local buckling test, some postbuckling strength is observed (i.e., the capacity is greater than the elastic critical local buckling), but this does not occur in the distortional buckling test. Failure mechanisms, as shown in Fig. 13, indicate reduced deformations in the web for the distortional buckling test. The distortional buckling tests on C sections generally exhibit many characteristics consistent with distortional buckling failures, but the response is more complicated than in the Z sections. This issue is discussed in further detail in the subsequent sections.

Failure Modes

Distortional Buckling

The "distortional buckling tests" referred to in this paper allow unrestrained distortional buckling to occur, but they do not guarantee this will happen. Local buckling and even lateral-torsional buckling may still initiate the failure in the distortional buckling tests. Of the 24 conducted tests 17 experienced failure mechanisms initiated by distortional buckling. A combination of visual inspection, recorded deformations, and supplementary finite element analyses were used to identify which buckling mode initiated the observed failure mechanism.

Finite element models consisting of shell elements were developed in *ABAQUS* (2001) to investigate the influence of the test setup on the buckling modes. Complete details of the finite element modeling, including additional nonlinear analysis modeling outside the scope of this paper, are provided in Yu (2005). For specimen 8C097 Figs. 14–16 present the predicted elastic buckling results for lateral-torsional, distortional, and local buckling, respectively. Numerical results for lateral-torsional (M_{crLTB}), distortional (M_{crd}), and local buckling ($M_{\mathrm{cr}\ell}$) from the finite element model are summarized for all the specimens in Table 5. The local and distortional buckling results may be compared with the pure cross-section analysis performed by the finite strip method, which ignores the finer details of the test setup, in Table 3. The testing details have only a small impact on the elastic buckling moments, on average the increase is less than 5%. The finite element models also indicate the lateral-torsional buckling moment is sufficiently

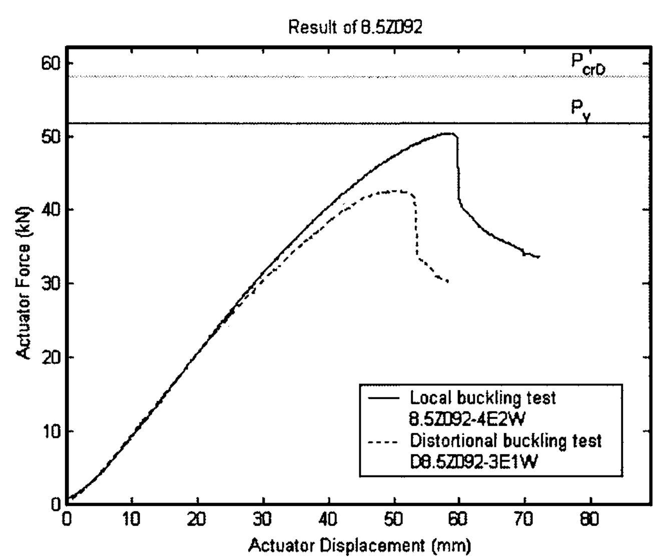

Fig. 10. Comparison of actuator force-displacement response for tests on 8.5Z092

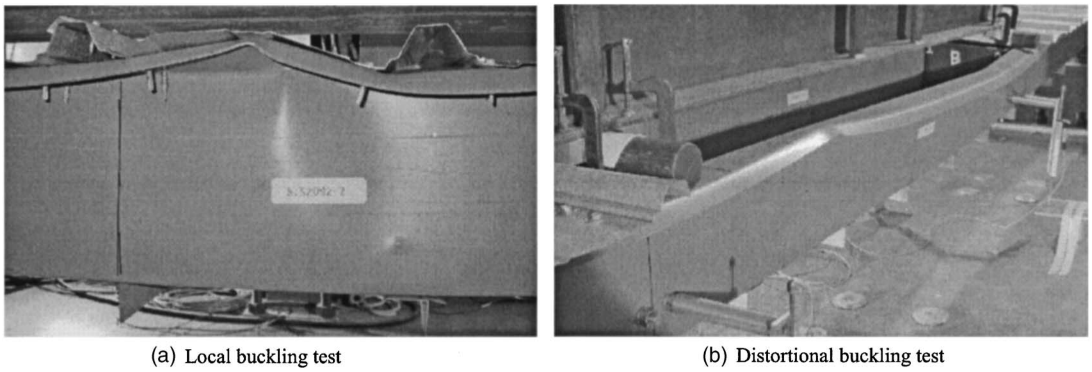

Fig. 11. Comparison of failure mechanisms for tests on 8.5Z092

increased, in all but specimen 8C097, which is discussed further below.

Based on the elastic buckling results, the Z section beams are anticipated to have failures initiated by distortional buckling, since $M_{\mathrm{crd}} < M_{\mathrm{cr}\ell}$ for all specimens. Indeed, visual inspection, recorded deformations, and observed strength all bear this out.

Previous work has shown that even when the elastic critical distortional buckling value is higher than the local buckling value ($M_{\mathrm{crd}} > M_{\mathrm{cr}\ell}$) the final failure mechanism may still be triggered by distortional buckling (Schafer and Peköz 1999; Schafer 2002). This is due in part to the fact that distortional buckling has lower postbuckling reserve, even in the inelastic regime. This finding was supported by the testing on C sections performed here. Distortional buckling is observed in specimens 8C068, 8C054, 8C043, 12C068, and 10C068 as shown in Fig. 17, even though $M_{\mathrm{crd}} > M_{\mathrm{cr}\ell}$. In general for the C sections, the web/flange juncture in the compression flange does not exhibit rotations as large as those observed in the Z sections. In the postpeak (past the peak bending moment) range of the tests, the majority of C sections exhibit rotation at the web/flange juncture, but in many cases translation and rotation of the entire section as well. This observation indicates a more complicated collapse response and the possible interaction of distortional buckling with local/lateral-torsional buckling in the C sections.

In the following sections, an examination of the seven tests which did not fail in mechanisms initiated by distortional buckling are presented. Failure in these seven other tests included: one by lateral-torsional buckling, one by material yielding, three by local buckling, one specimen with large pretest damage, and one by shear + bending interaction.

Lateral-Torsional Buckling

As shown in Table 5, D8C097-5E4W is the only test specimen which has a lower lateral-torsional buckling moment than that of local or distortional buckling. In the test, shown in Fig. 18, significant twist of the specimens occurred. Subsequently, an additional angle was attached to the compression flange at midspan and another test performed (D8C097-7E6W) as shown in Fig. 19. The new test exhibited the same initial elastic stiffness and sustained a significantly higher load before failure occurred, as shown in Fig. 20. The large twist that occurred in the first test was removed in the subsequent test, as shown in Fig. 21. In the modified test (D8C097-7E6W) failure occurred due to distortional buckling. D8C097-5E4W, which provides an examination of the role of lateral-torsional buckling, is not considered a distortional buckling test for the purposes of this paper, and is not used in comparison to the design specifications.

Material Yielding

Test D3.62C054-3E4W failed by material yielding. The beam's yield moment is 3.8 kN m and the distortional buckling moment is 7.4 kN m. The observed peak moment was also 3.8 kN m and no deformations consistent with distortional buckling were observed prior to obtaining the peak moment. The beam showed significant nonlinearity, but no sharp strength loss during the loading process, as shown in Fig. 8.

Local Buckling

Failures initiated by local buckling were visually observed in three tests: D8C045-1E2W, D8C033-1E2W, and D10C056-3E4W, as shown in Figs. 22–24. Failure in these three tests is categorized with the previously performed local buckling tests. In

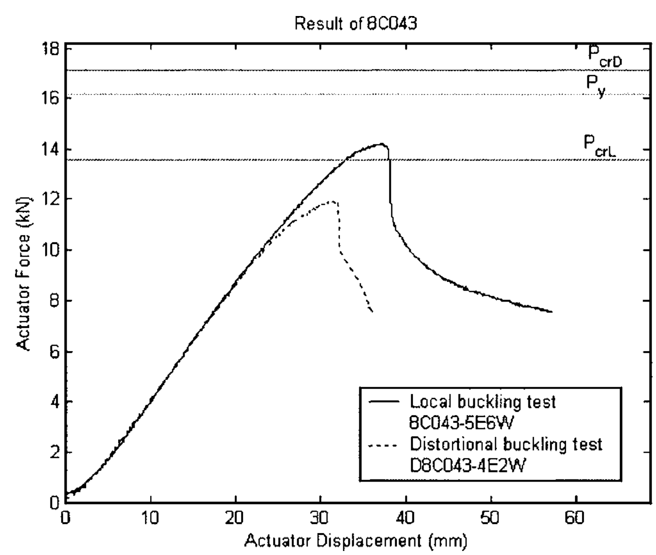

Fig. 12. Comparison of actuator force-displacement response for tests on 8C043

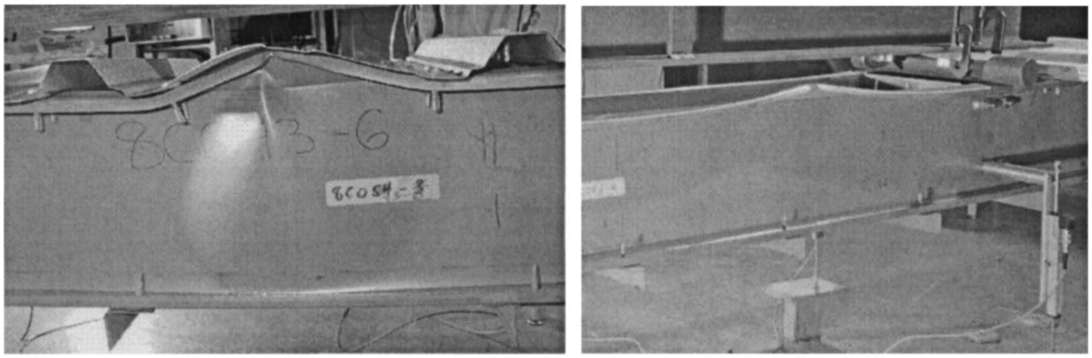

(a) Local buckling test (b) Distortional buckling test

Fig. 13. Comparison of failure mechanisms for tests on 8C043

addition, according to direct strength method (AISI 2004, Appendix 1) predictions these three specimens have lower local buckling strength than distortional buckling strength.

Pretest Damage

Test D12C068-1E2W had a dent in the compression flange prior to testing, which initiated the failure during testing. The observed strength is significantly lower than predictions by design specifications: 23% off the direct strength method (AISI 2004, Appendix 1) prediction and 30% off AISI (2001). This mildly damaged specimen was examined in greater detail with the use of nonlinear finite element models in Yu (2005). For comparison to design specifications this specimen is not included in the summary statistics.

Shear + Bending Interaction

Failure in test D8.5Z059-6E5E (the thinnest of the Z members tested) occurred outside of the constant moment region. Initial geometric imperfections, uneven specimen setup, and shear and bending interaction are possible reasons for the unexpected failure mode. In all other tests, the tube section bolting the beams together provided sufficient restraint to force the failure inside the constant moment region. For comparison to design specifications this specimen is not included in the summary statistics.

Comparison with Design Specifications

Six design methods are considered for comparison: U.S. (AISI 1996); Canada (CSA 1994); Australia/New Zealand (AS/NZS 1996); North America (AISI 2001); Europe (CEN 2002); and the recently adopted direct strength method (Schafer and Peköz 1998; AISI 2004, Appendix 1). DSM prediction equations for both local and distortional buckling of beams are briefly summarized here. For local buckling the capacity is

$$\lambda_\ell \leqslant 0.776, \quad M_{\mathrm{DS}\ell} = M_{ne} \tag{1}$$

$$\lambda_\ell > 0.776, \quad M_{\mathrm{DS}\ell} = \left[1 - 0.15\left(\frac{M_{\mathrm{cr}\ell}}{M_{ne}}\right)^{0.4}\right]\left(\frac{M_{\mathrm{cr}\ell}}{M_{ne}}\right)^{0.4} M_{ne} \tag{2}$$

$$\lambda_\ell = \sqrt{M_{ne}/M_{\mathrm{cr}\ell}} \tag{3}$$

where $M_{\mathrm{cr}\ell}$=critical elastic local buckling moment; and M_{ne}=moment capacity due to lateral-torsional buckling. Since the beams are assumed to be laterally braced $M_{ne}=M_y$, where M_y=moment at first yield.

For distortional buckling the capacity is

$$\lambda_d \leqslant 0.673, \quad M_{\mathrm{DSd}} = M_y \tag{4}$$

$$\lambda_d > 0.673, \quad M_{\mathrm{DSd}} = \left[1 - 0.22\left(\frac{M_{\mathrm{crd}}}{M_y}\right)^{0.5}\right]\left(\frac{M_{\mathrm{crd}}}{M_y}\right)^{0.5} M_y \tag{5}$$

$$\lambda_d = \sqrt{M_y/M_{\mathrm{crd}}} \tag{6}$$

where M_{crd}=critical elastic distortional buckling moment.

A summary of the test-to-analytically predicted capacities for all six design methods, for both the local and distortional buckling series of tests, is given in Table 6. Results for individual tests are provided in Table 3. On average, all six methods provide reliable strength predictions for the local buckling tests. The direct strength method (DSM) uses a single strength curve for each buckling mode and gross section properties, while the other five methods apply effective width concepts.

For distortional buckling, only AS/NZS, EN1993, and DSM have specific methodologies. AS/NZS and DSM employ the minimum of separate local and distortional buckling strength predictions while EN1993 assumes distortional buckling is a reduction to be applied in addition to local buckling. Table 6 shows that AS/NZS, EN1993, and DSM provide reasonable strength predictions for the distortional buckling failures, though EN1993 still remains about 4% unconservative on average. AS/NZS and DSM

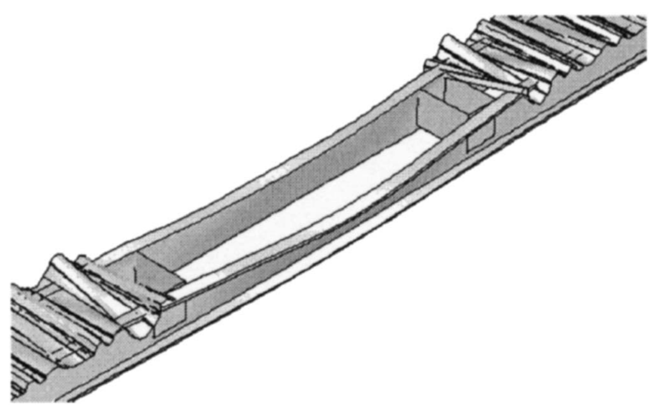

Fig. 14. Finite element prediction for lateral-torsional buckling mode of beam D8C097-5E4W

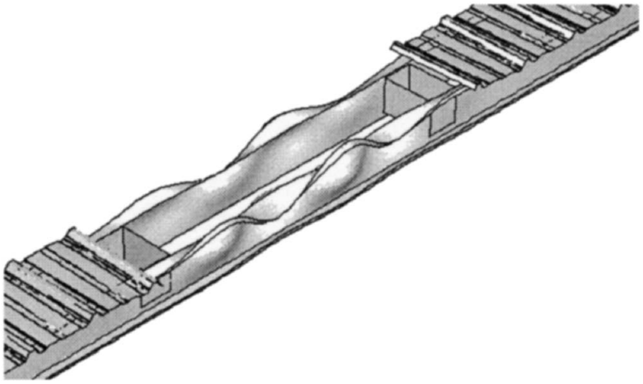

Fig. 15. Finite element prediction for distortional buckling mode of beam D8C097-5E4W

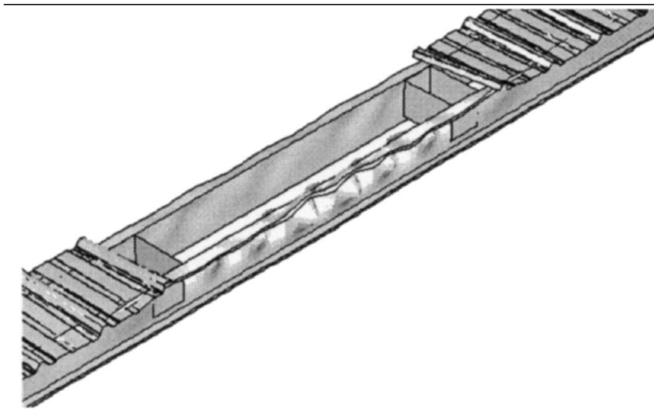

Fig. 16. Finite element prediction for local buckling mode of beam D8C097-5E4W

Table 5. Elastic Buckling Moments of Performed Tests using *ABAQUS* Model with all Testing Details

Test label	$M_{cr\ell}$ (kN m)	M_{crd} (kN m)	M_{crLTB} (kN m)
D8.5Z120-4E1W	171.8	87.2	137.7
D8.5Z115-1E2W	>163.9	81.3	132.6
D8.5Z092-3E1W	77.3	50.8	84.4
D8.5Z082-4E3W	56.6	39.8	>63.9
D8.5Z065-7E6W	28.6	23.8	>34.1
D8.5Z065-4E5W	23.3	19.6	>26.0
D8.5Z059-6E5W	24.6	20.7	>28.8
D11.5Z092-3E4W	71.6	52.4	>85.9
D11.5Z082-3E4W	56.5	43.5	>68.7
D8C097-5E4W	89.9	68.9	60.3
D8C085-2E1W	50.9	44.8	>52.9
D8C068-6E7W	33.2	31.6	>38.2
D8C054-7E6W	13.2	14.6	>16.3
D8C045-1E2W	4.1	>4.8	>4.8
D8C043-4E2W	9.7	>12.1	>12.1
D8C033-1E2W	3.7	>4.7	>4.7
D12C068-1E2W	22.8	23.5	>28.9
D12C068-10E11W	20.7	21.4	>26.2
D10C068-4E3W	20.8	21.0	>25.6
D10C056-3E4W	15.8	>18.7	>18.7
D10C048-1E2W	10.0	>10.0	>10.0
D6C063-2E1W	20.4	18.4	>21.5
D3.62C054-3E4W	>13.6	7.5	10.6

Note: Lower bounds are given to those modes which are not included in the first 30 eigenmodes calculated in the *ABAQUS* analysis. Each model includes two specimens, and is thus approximately double the results of Table 3.

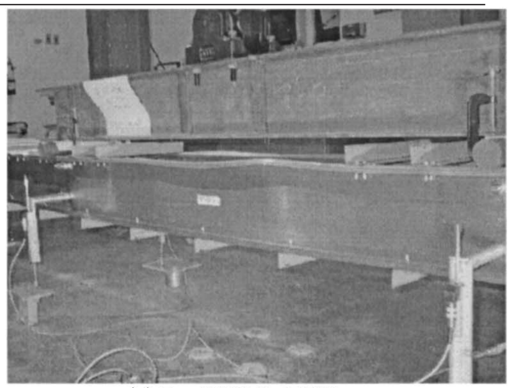

(a) Test D8C068-6E7W

(b) Test D8C054-7E6W

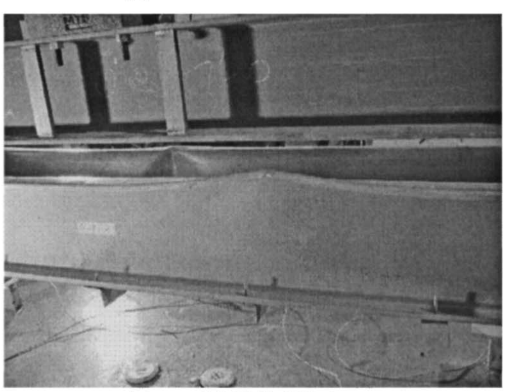

(c) Test D8C043-4E2W

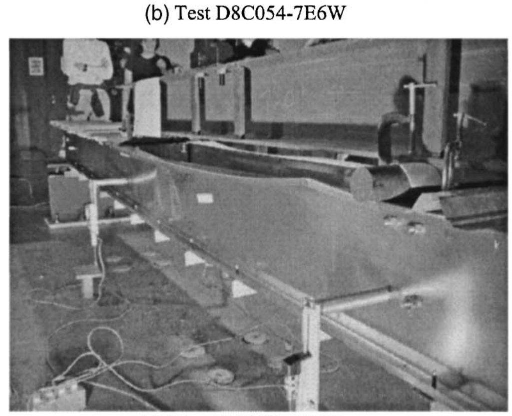

(d) Test 10C068-4E3W

Fig. 17. Observed distortional buckling deformations and failure mechanisms in C sections even when elastic critical local buckling is at a lower moment than distortional buckling ($M_{cr\ell} < M_{crd}$)

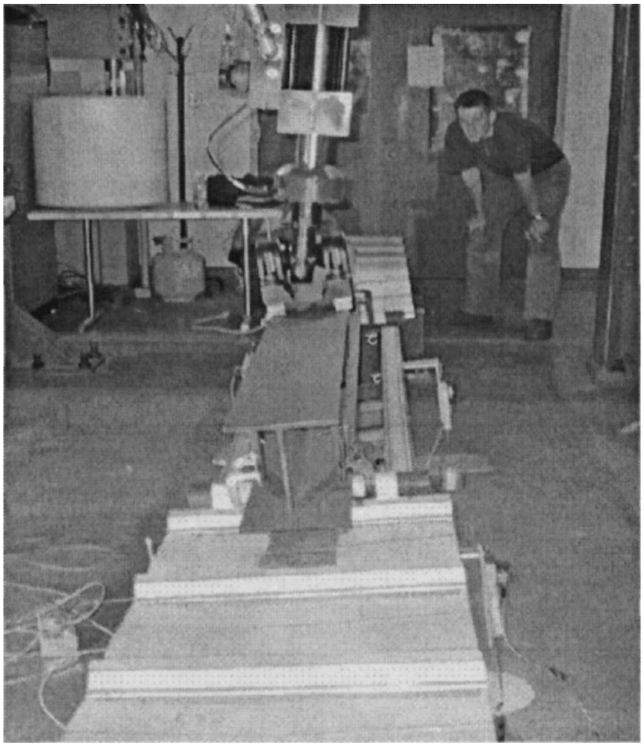

Fig. 18. Lateral-torsional buckling observed in test D8C097-5E4W

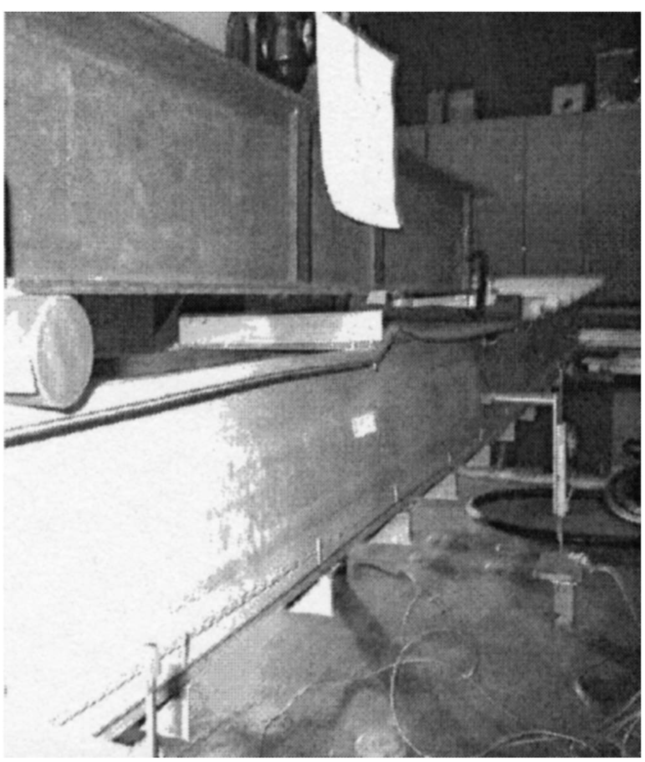

Fig. 19. Distortional buckling observed in re-rest of D8C097-7E6W, note added angle at midspan

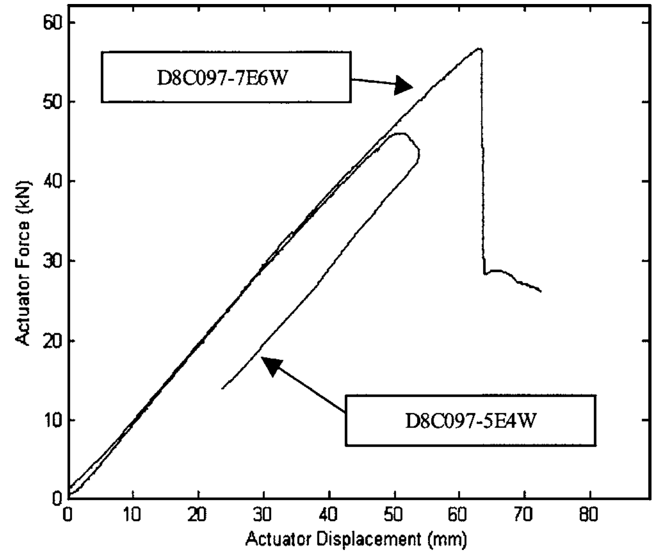

Fig. 20. Actuator force-displacement response for tests on D8C097

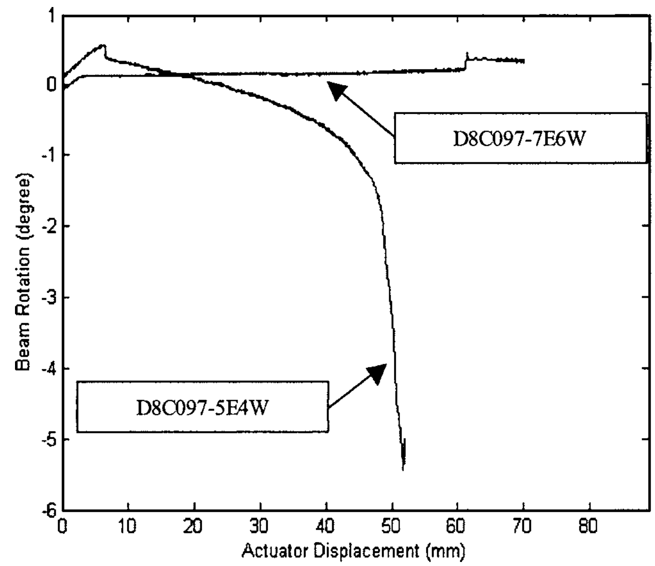

Fig. 21. Beam rotation at the south loading point for tests on D8C097

Fig. 22. Local failure observed in test D8C045-1E2W

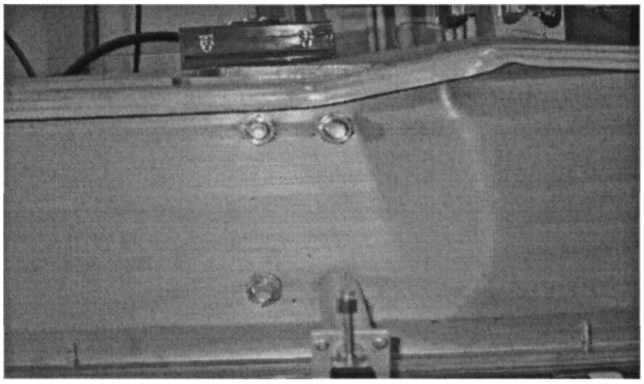

Fig. 23. Local failure observed in test D8C033-1E2W

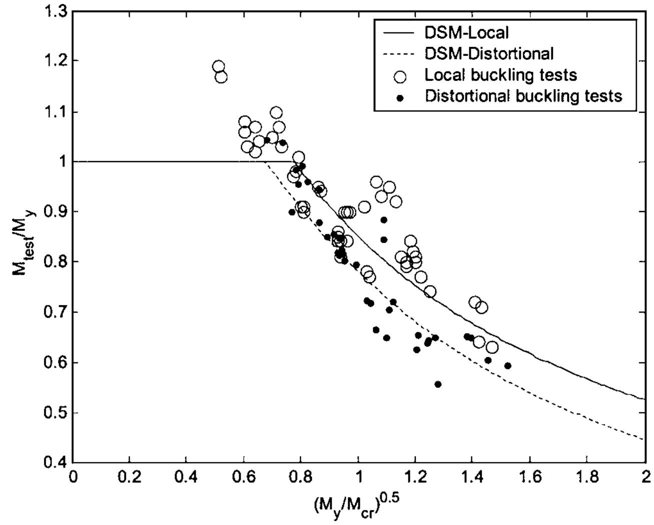

Fig. 25. Comparison of direct strength method prediction equations with test results

employ the same basic procedure and are quite similar for distortional buckling strength prediction. AS/NZS and DSM provide a test-to-predicted ratio closest to 1 and have the lowest coefficient of variation. AISI, S136, and NAS provide systematically unconservative predictions for the distortional buckling strength, with an average error between 8 and 15%.

DSM provides good agreement with the results of both series of tests. Fig. 25 provides a graphical representation of the DSM predictions, in the figure M_{cr} represents $M_{cr\ell}$ for the local buckling tests and M_{crd} for the distortional buckling tests. Prediction of the local buckling capacity exhibits less scatter than the distortional buckling capacity. The DSM strength equations were calibrated to other tests, including a variety of cross sections beyond C and Z sections as summarized in (AISI 2004, Appendix 1). The reliable performance of DSM with the test data presented here serves as additional validation for DSM.

Discussion

Design can account for the worst-case scenario for distortional buckling with simple equations such as those used in AS/NZS (1996) or DSM (AISI 2004, Appendix 1) if the elastic distortional buckling moment (M_{crd}) is known. However, without computer methods such as finite strip analysis, calculation of M_{crd} is nontrivial. The writers are working on simplified M_{crd} calculations for use in preliminary design, but simple, general, and accurate procedures remain elusive.

Fig. 24. Local failure observed in test D10C056-3E4W

One alternative to traditional design methods is to perform testing to determine the distortional buckling strength. As these experiments show, generalized protocols for performing the tests are not easy to arrive at. Thicker specimens tend to have both elevated local and distortional buckling stress and can thus readily be controlled by lateral-torsional buckling, or yielding. Thinner specimens may also be controlled by other limit states, including local buckling and shear and bending interaction. While these failure modes were relatively uncommon in our tests, they were all observed, and serve to demonstrate the variety of behavior that may occur even at modest unbraced lengths.

Testing performed herein is a worst-case scenario for distortional buckling: (1) there is no restraint of the compression flange, (2) the demand is pure bending, and (3) lateral-torsional buckling is restricted. Restraint of the compression flange is a key issue, if restraint does not exist distortional buckling is likely to initiate the failure at levels much below that of local buckling. The case of partial restraint is examined experimentally in Yu and Schafer (2003). Further testing, analysis, and design procedures are needed to incorporate this influence in design. The pure bending demand used in the testing setup does not allow for an exploration of the influence of moment gradient on the distortional buckling capacity. Since the distortional buckling half-wavelength is relatively long, moment gradients will have an influence on the distortional buckling capacity. Finally, if a beam is not braced, lateral-torsional buckling will often occur far in advance of distortional buckling, and will control the design. Issues related to partial restraint and moment gradient in distortional buckling of cold-formed steel beams have been recently examined in Yu (2005) and will be the subject of future papers by the writers.

Conclusions

Four-point bending tests on a wide variety of industry standard, laterally braced C and Z section beams where the compression flange is unrestrained in the constant moment span over a distance of 1,626 mm (64 in.) indicate that distortional buckling is the most likely failure mode. Distortional failures occur even when local buckling is at a lower critical elastic moment than distortional buckling. Laterally braced C and Z sections which are free

Table 6. Summary of Test-to-Predicted Ratios for Existing and Proposed Design Methods

			$M_{\text{test}}/M_{\text{AISI}}$	$M_{\text{test}}/M_{\text{S136}}$	$M_{\text{test}}/M_{\text{NAS}}$	$M_{\text{test}}/M_{\text{AS/NZS}}$	$M_{\text{test}}/M_{\text{EN1993}}$	$M_{\text{test}}/M_{\text{DSM}}$
Local buckling tests	Controlling specimens	μ	1.01	1.06	1.02	1.01	1.01	1.03
		σ	0.04	0.04	0.05	0.04	0.06	0.06
	Second specimens	μ	1.00	1.05	1.01	1.00	1.01	1.04
		σ	0.05	0.06	0.07	0.05	0.06	0.07
Distortional buckling tests	Controlling specimens	μ	0.86	0.92	0.88	1.02	0.96	1.02
		σ	0.08	0.08	0.09	0.07	0.09	0.07
	Second specimens	μ	0.85	0.90	0.87	1.00	0.94	1.00
		σ	0.07	0.07	0.09	0.07	0.09	0.07

Note: μ=average; and σ=standard deviation.

to fail in distortional buckling result in an average loss of 17% of their bending capacity when compared with the same section where distortional buckling is restrained and failure occurs due to local buckling. Previous testing by Yu and Schafer (2003) demonstrated that if additional rotational restraint can be provided to the compression flange, such as through engagement of a through-fastened deck, the distortional buckling mode can be avoided and a local buckling mode triggered instead.

Comparison of the experimental results with design specifications indicate that the American Specification (AISI 1996) and Canadian Standard (CSA 1994) as well as the newly adopted North American Specification (AISI 2001) provide a poor prediction of the strength for members with failures initiated by distortional buckling. Errors are, on average, 8–15% unconservative for these design specifications. Eurocode (CEN 2002) which provides additional measures to account for distortional buckling is, on average, 4% unconservative. Two methods which include explicit procedures for distortional buckling, the Australian/New Zealand standard (AS/NZS 1996) and the Direct Strength Method (AISI 2004, Appendix 1), provide reliable predictions of the capacity in distortional buckling with conservative errors of, on average, 2%. The test data provides validation for the Direct Strength Method predictor equations, and these equations are recommended for use in design.

Acknowledgments

The sponsorship of the American Iron and Steel Institute (AISI) for both phases of this work, and the Metal Building Manufacturers Association for the first phase is gratefully acknowledged. Donation of materials by Varco-Pruden, Clark Steel, and Dietrich Design Group is also gratefully acknowledged. The assistance of the AISI task group in developing the testing plan is appreciated. Don Johnson, Maury Golovin, Joe Nunnery, Joe Wellinghoff, and Steve Thomas have all been helpful with their ideas and generous with their time. Special thanks go to Sandor Ádány from Budapest University of Technology and Economics, who helped on the Eurocode calculation. The experiments would not have been possible without the help of Johns Hopkins undergraduates: Liakos Ariston, Brent Bass, Andrew Myers, Sam Phillips, and Tim Ruth. Sam's work during Phase 1 and Tim's during Phase 2 was particularly helpful. Finally, the work has been skillfully aided by our laboratory technician Jack Spangler, and our machinist Jim Kelly.

Notation

The following symbols are used in this paper:

b = flange width;
b_c = out-to-out compression flange width;
b_t = out-to-out tension flange width;
b_1, b_2 = effective width of the compressive portions of the web;
b_{comp} = depth of the full compression portion of the web;
d = flange lip width;
d_c = out-to-out compression flange lip stiffener length;
d_t = out-to-out compression flange lip stiffener length;
E = modulus of elasticity;
f_{cr} = critical buckling stress;
f_u = ultimate stress capacity;
f_y = yield stress;
h = out-to-out web depth;
M_{AISI} = AISI (1996) predicted flexural capacity;
$M_{\text{AS/NZS}}$ = AS/NZS (1996) predicted flexural capacity;
M_{crd} = elastic critical distortional buckling moment;
$M_{\text{cr}\ell}$ = elastic critical local buckling moment;
M_{crLTB} = elastic critical lateral-torsional buckling moment;
M_{DSd} = DSM predicted flexural capacity for distortional buckling;
$M_{\text{DS}\ell}$ = DSM predicted flexural capacity for local buckling;
M_{DSM} = minimum value of M_{DSd} and M_{DSl};
M_{EN1993} = EN1993 (CEN 2002) predicted flexural capacity;
M_{NAS} = NAS (AISI 2001) predicted flexural capacity;
M_{S136} = S136 (CSA 1994) predicted flexural capacity;
M_{test} = tested flexural capacity;
M_y = yield moment;
P_{crD} = actuator load leads to critical elastic distortional buckling;
P_{crL} = actuator load leads to critical elastic distortional buckling;
P_{D} = actuator load leads to distortional buckling capacity;
P_{L} = actuator load leads to local buckling capacity;
P_y = actuator load leads to yield meoment;
r_{dc} = outer radius between compression flange and lip;

r_{dt} = outer radius between tension flange and lip;
r_{hc} = outer radius between web and compression flange;
r_{ht} = outer radius between web and tension flange;
t = base metal thickness;
θ_c = compression flange stiffener angle from horizontal; and
θ_t = tension flange stiffener angle from horizontal.

References

ABAQUS version 6.2.; users manual. (2001) ABAQUS, Inc., Pawtucket, R.I., (www.abaqus.com).

American Iron and Steel Institute (AISI). (1996). *Specification for the design of cold-formed steel structural members*, Washington, D.C.

American Iron and Steel Institute (AISI). (2001). *North American specification for the design of cold-formed steel structural members*, Washington, D.C.

American Iron and Steel Institute (AISI). (2004). *Supplement 2004 to the North American specificaiton for the design of cold-formed steel structural members, 2001 edition, Appendix 1, design of cold-formed steel structural members using direct strength method*, Washington, D.C.

American Society for Testing and Materials (ASTM). (2000). *E8-00, Standard test methods for tension testing of metallic material*, Philadelphia.

Canadian Standards Association (CSA). (1994). *Cold-formed steel structural members S136-94*, Ontario, Canada.

Desmond, T. P., Peköz, T., and Winter, G. (1981). "Edge stiffeners for thin-walled members." *J. Struct. Div. ASCE*, 107(2), 329–353.

Comité Européen de Normalisation (CEN). (2002). "Eurocode 3: Design of steel structure." *European Standard EN1993-1-3*, CEN, Brussels, Belgium.

Hancock, G. J. (1997). "Design for distortional buckling of flexural members." *Thin-Walled Struct.*, 27(1), 3–12.

Hancock, G. J., Rogers, C. A., and Schuster, R. M. (1996). "Comparison of the distortional buckling method for flexural members with tests." *13th Int. Specialty Conf. on Cold-Formed Steel Structures*, 125–140, St. Louis.

Schafer, B. W. (2005). *CUFSM 2.6: Elastic buckling analysis of thin-walled members by finite strip analysis*, (www.ce.jhu.edu/bschafer/cufsm).

Schafer, B. W. (2002). "Local, distortional, and Euler buckling in thin-walled columns." *J. Struct. Eng.*, 128(3), 289–299.

Schafer, B. W., and Peköz, T. (1998). "Direct strength prediction of cold-formed steel members using numerical elastic buckling solutions." *14th Int. Specialty Conf. on Cold-Formed Steel Structures*, St. Louis.

Schafer, B. W., and Peköz, T. (1999). "Laterally braced cold-formed steel flexural members with edge stiffened flanges." *J. Struct. Eng.* 125(2), 118–127.

Schafer, B. W., and Trestain, T. (2002). "Interim design rules for flexure in cold-formed steel webs." *16th Int. Specialty Conf. on Cold-Formed Steel Structures*, Orlando, Fla.

Silvestre, N., and Camotim, D. (2004). "Distortional buckling formulae for cold-formed steel C and Z-section members: Part I—Derivation." *Thin-Walled Struct.*, 42(11), 1567–1597.

Standards Australia and the Australian Institute of Steel Construction (AS/NZS). (1996). *AS/NZS 4600: 1996 Cold-Formed Steel Structures*.

Yu, C. (2005). "Distortional buckling of cold-formed steel members in bending." Ph.D. dissertation, Johns Hopkins Univ., Baltimore.

Yu, C., and Schafer, B. W. (2003). "Local buckling test on cold-formed steel beams." *J. Struct. Eng.*, 129(12), 1596–1606.